Contrib Mineral Petrol (2007) 153:139–157
DOI 10.1007/s00410-006-0144-x

ORIGINAL PAPER

Coupling of oceanic and continental crust during Eocene eclogite-facies metamorphism: evidence from the Monte Rosa nappe, western Alps

Thomas J. Lapen · Clark M. Johnson · Lukas P. Baumgartner · Giorgio V. Dal Piaz · Susanne Skora · Brian L. Beard

Received: 1 May 2006 / Accepted: 1 September 2006 / Published online: 21 November 2006

Abstract High precision U–Pb geochronology of rutile from quartz–carbonate–white mica–rutile veins that are hosted within eclogite and schist of the Monte Rosa nappe, western Alps, Italy, indicate that the Monte Rosa nappe was at eclogite-facies metamorphic conditions at 42.6 ± 0.6 Ma. The sample area [Indren glacier, Furgg zone; Dal Piaz (2001) Geology of the Monte Rosa massif: historical review and personal comments. SMPM] consists of eclogite boudins that are exposed inside a south-plunging overturned synform within micaceous schist. Associated with the eclogite and schist are quartz–carbonate–white mica–rutile veins that formed in tension cracks in the eclogite and along the contact between eclogite and surrounding schist. Intrusion of the veins at about 42.6 Ma occurred at eclogite-facies metamorphic conditions (480–570°C, >1.3–1.4 GPa) based on textural relations, oxygen isotope thermometry, and geothermobarometry. The timing of eclogite-facies metamorphism in the Monte Rosa nappe determined in this study is identical to that of the Gran Paradiso nappe [Meffan-Main et al. (2004) J Metamorphic Geol 22:261–281], confirming that these two units have shared the same Alpine metamorphic history. Furthermore, the Gran Paradiso and Monte Rosa nappes underwent eclogite-facies metamorphism within the same time interval as the structurally overlying Zermatt-Saas ophiolite [~50–40 Ma; e.g., Amato et al. (1999) Earth Planet Sci Lett 171:425–438; Mayer et al. (1999) Eur Union Geosci 10:809 (abstract); Lapen et al. (2003) Earth Planet Sci Lett 215:57–72]. The nearly identical *P–T–t* histories of the Gran Paradiso, Monte Rosa, and Zermatt-Saas units suggest that these units shared a common Alpine tectonic and metamorphic history. The close spatial and temporal associations between high pressure (HP) ophiolite and continental crust during Alpine orogeny indicates that the HP internal basement nappes in the western Alps may have played a key role in exhumation and preservation of the ophiolitic rocks through buoyancy-driven uplift. Coupling of oceanic and continental crust may therefore be critical in preventing permanent loss of oceanic crust to the mantle.

Communicated by: J. Hoefs.

T. J. Lapen · C. M. Johnson · B. L. Beard
Department of Geology and Geophysics,
University of Wisconsin, Madison, WI, USA

L. P. Baumgartner · S. Skora
Institute of Mineralogy and Petrology,
University of Lausanne, Lausanne, Switzerland

G. V. D. Piaz
Department of Geology, Paleontology and Geophysics,
University of Padova, Padova, Italy

T. J. Lapen (✉)
Department of Geosciences, Science and Research 1,
University of Houston, 4800 Calhoun Rd, Houston,
TX 77204, USA
e-mail: tjlapen@uh.edu

Introduction

In recent years, rapidly exhumed high- and ultra high-pressure (HP-UHP) metamorphic units have been recognized in convergent orogens worldwide (e.g., Amato et al. 1999; Rubatto and Hermann 2001; Carswell et al. 2003; Hacker et al. 2003), most commonly associated with continent–continent collisional mar-

gins. Subduction of continental crust to HP-UHP conditions requires overcoming density contrasts that are unfavorable to deep burial and preservation of HP-UHP assemblages that formed deep within subduction zones require rapid exhumation. The occurrence of HP-UHP terranes, therefore, bears on geodynamic models of convergent plate margins.

The western Alps (Fig. 1) are a classic subduction-related, continent–continent collisional orogen. The core of the belt represents a fossil subduction complex (Austroalpine-Penninic wedge) that was developed before and during continental collision. Large fragments of low-density continental crust were deeply subducted and then exhumed together with ophiolitic remnants of the consumed oceanic crust (Ernst 1971; Dal Piaz et al. 1972). Petrologic estimates show that these units were variously buried to depths >30–40 km (in some cases ≥100 km), as clearly documented by blueschist- and eclogite-facies assemblages (Frey et al. 1974, 1976; Compagnoni et al. 1977; Bigi et al. 1990; Spalla et al. 1996; Oberhänsli et al. 2004) that are locally coesite bearing (Dora Maira nappe; Chopin 1984; Zermatt-Saas ophiolite at Lago di Cignana; Reinecke 1991).

The western Alps contain some of the world's most rapidly exhumed HP-UHP rocks that include both oceanic and continental protoliths. Following initial pioneering work (Dal Piaz et al. 1972; Gosso et al. 1979), there have been a growing number of studies aimed at evaluating and understanding the rate of exhumation (e.g., Amato et al. 1999; Rubatto and Hermann 2001), as well as the mechanisms involved

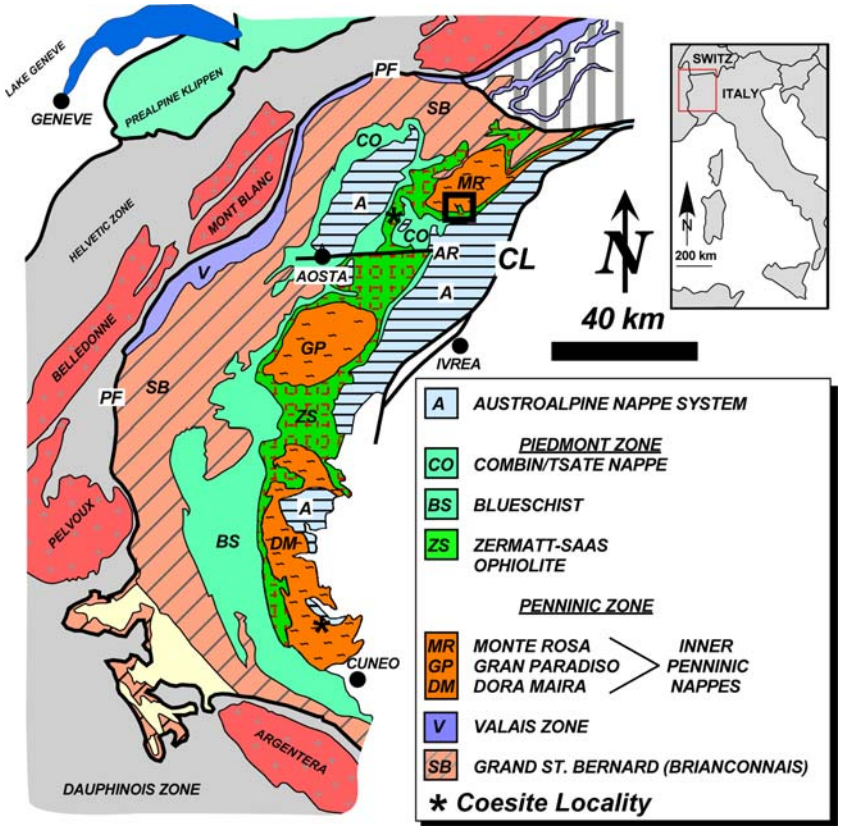

Fig. 1 Generalized geologic map of the western Alps (after Dal Piaz 1999). The study area is located on the southern margin of the Monte Rosa nappe (*MR*) and is indicated by a *box*. The Helvetic and Dauphinois zones as well as units colored *red* with *gray* crosses represent deformed European cover rocks, and folded and warped continental basement, respectively. The Valais zone represents oceanic rocks of supposedly Cretaceous age (Stampfli and Marchant 1997) or of Early Carboniferous age (Bussy et al. 2005). Oceanic units of the ophiolitic Piedmont Zone [Combin (BS/CO) and Zermatt-Saas ophiolite nappes (*ZS*)] represent material from the Jurassic Piedmont-Ligurian Ocean situated between the European passive continental margin (Monte Rosa-Gran Paradiso and Grand St. Bernhard nappes and the African/Apulian promontory represented by the Austroalpine nappes (*A*). The internal Penninic nappes [Dora Maira (*DM*), Gran Paradiso (*GP*), and Monte Rosa (*MR*)] are structurally beneath the Zermatt-Saas ophiolite and are exposed as domal structures along the strike of the orogen. *Thick lines* represent large-scale structures (thrust and major faults; *PF* Penninic frontal thrust, *CL* Canavese fault system, *AR* Aosta-Ranzola fault system)

(e.g., Wheeler 1991; Spalla et al. 1996; Escher and Beaumont 1997; Reddy et al. 1999, 2003; Engi et al. 2001b; Schwartz et al. 2001; Kurz and Froitzheim 2002). These studies generally call upon buoyancy-driven processes to explain the rapid exhumation of HP-UHP rocks. The potential role of low-density material in exhuming HP-UHP units is critical, but clear linkages among the lithologically diverse HP-UHP terranes remain incomplete.

The age of eclogite-facies metamorphism of low-density, continental cover and/or basement nappes in the western Alps is important for testing models where such units provided density-assisted exhumation of HP-UHP ophiolitic units. Such age constraints have, however, been quite difficult to obtain due to uncertainties in relating dated mineral phases to the HP-UHP conditions, as well as complications associated with age inheritance in Paleozoic-age continental units (see Dal Piaz 2001, for a further discussion). Despite intensive study, it remains unclear if major continental components of the Alpine orogen were subducted together as a coherent tract or were subducted and exhumed diachronously, before, during, or after subduction of oceanic crust. This ambiguity in the age and duration of subduction-related metamorphism of the continental basement nappes greatly hinders development of coherent geodynamic models of oceanic and continental subduction and exhumation in the western Alps.

In this paper, we present new high precision U–Pb ages of rutile and *P–T* data of the Alpine eclogite-facies metamorphism in the Penninic Monte Rosa nappe, Gressoney Valley, Italy. Our results indicate that both the Monte Rosa nappe and the overlying Zermatt-Saas ophiolite were at eclogite-facies metamorphic conditions at similar times. Furthermore, because of their close spatial association (Fig. 1), they were also likely to have been adjacent to each other from eclogite-facies conditions to their present configuration at the surface. These relations support the hypothesis that the relatively low-density Monte Rosa nappe may have aided in the exhumation of the structurally overlying Zermatt-Saas ophiolite.

Background geology and geochronology

The western Alps record Cretaceous to present convergence between the Adriatic (African) continental upper plate and the subducting lower plate, which included the Mesozoic Piedmont Ocean and the European passive continental margin. Surface geology and deep seismic experiments show that the Austroalpine-Penninic wedge is a stack of thin, primarily continental crustal nappes that overlie the current European lithospheric lower plate, indented by the Adriatic (southern Alps) lithosphere (e.g., Roure et al. 1990; Pfiffner et al. 1997; Dal Piaz et al. 2003). From top to bottom and from the inner (SE) to the outer (NW) zones, the Austroalpine-Penninic wedge mainly consists of: (1) the Adria-derived Austroalpine nappe system, which developed in the Late Cretaceous before closure of the Piedmont-Ligurian Ocean; (2) the ophiolitic Piedmont zone, a structurally composite system that includes the Combin zone and underlying Zermatt-Saas ophiolite; (3) the Penninic zone, which is a stack of collisional nappes that were accreted during the Paleogene and were derived from the ocean-facing edge of the European continental margin. The Penninic zone includes the inner/upper Penninic Monte Rosa–Gran Paradiso–Dora Maira nappes, and the mid-Penninic Grand St. Bernard nappe system (Fig. 1; see Dal Piaz et al. 1972, 2003; Dal Piaz and Ernst 1978; Ballèvre et al. 1986; Coward and Dietrich 1989; Michard et al. 1996; Escher et al. 1997; Stampfli and Marchant 1997).

Initiation of subduction in the western Alpine domain is not well known, although the occurrence of orogenic clastic deposits that overlie oceanic sequences suggests an Early or mid-Cretaceous age. A cool, subduction-related thermal regime was present in the Late Cretaceous (~70–75 Ma), as evidenced by the age of eclogite- and blueschist-facies metamorphism in the Austroalpine Sesia-Lanzo Zone (Inger et al. 1996) and Dent Blanche (Pillonet) thrust system (Cortiana et al. 1998). Early work interpreted HP metamorphism associated with subduction of the Piedmont Zone (e.g., Zermatt-Saas ophiolite complex) and Inner Penninic nappes (e.g., Dora Maira, Gran Paradiso, and Monte Rosa nappes) as beginning in the Cretaceous (90–65 Ma) based on K–Ar, Ar–Ar, and U–Pb geochronology (e.g., Hunziker 1974; Bocquet et al. 1974; Chopin and Monié 1984; Paquette et al. 1989). Recent geochronological work in the Zermatt-Saas ophiolite, however, indicates that this crustal subduction event was most pronounced in Eocene time, as indicated by SHRIMP U–Pb zircon, Sm–Nd, Rb–Sr, Ar–Ar, and Lu–Hf geochronology (e.g., Bowtell et al. 1994; Rubatto et al. 1998; Amato et al. 1999; Mayer et al. 1999; Dal Piaz et al. 2001; Lapen et al. 2003). These new age data have provided the best constraints for the age and duration of HP-UHP metamorphism of the ophiolitic units.

The age and duration of eclogite-facies metamorphism in the Gran Paradiso and Monte Rosa continental nappes that underlie the oceanic units, however,

are less well constrained. The complex polyphase metamorphic history of these nappes (Bearth 1952; 1958; Hunziker 1970; Frey et al. 1976; Dal Piaz 1971; Dal Piaz and Lombardo 1986; Borghi et al. 1996), as well as the general difficulty in achieving chemical and isotopic equilibrium between minerals during Alpine metamorphism (e.g., Frey et al. 1976), complicates efforts to obtain reliable ages of eclogite-facies metamorphism. Efforts to date the HP metamorphism in these basement nappes by $^{40}Ar/^{39}Ar$ has yielded mid-Cretaceous ages (e.g., Chopin and Maluski 1980; Chopin and Monié 1984), but these ages may be complicated by the presence of excess Ar (e.g., Chopin and Monié 1984; Arnaud and Kelley 1995; Ruffet et al. 1997; Pawlig et al. 2001). The Cretaceous $^{40}Ar/^{39}Ar$ ages for HP micas stand in contrast to ages derived from other isotope systems that may be less susceptible to inherited components. For example, Rb–Sr geochronology in the Gran Paradiso nappe yielded an apatite-phengite age for HP metamorphism of 43.0 ± 0.5 Ma (Meffan-Main et al. 2004). Estimates of the age of HP metamorphism in the Monte Rosa nappe are 40–35 Ma for U–Pb in monazite (Engi et al. 2001a) and 34.9 ± 1.4 Ma for a SHRIMP U–Pb zircon age (Rubatto and Gebauer 1999). It is important to note, however, that the youngest ages of ~35 Ma cannot reflect the age of HP metamorphism because they lie in conflict with zircon fission-track ages in the region that record cooling through ~250°C (Hurford and Hunziker 1989; Hurford et al. 1991) at ~30–35 Ma.

Exhumation of both the eclogite-facies Zermatt-Saas ophiolite and the Monte Rosa–Gran Paradiso basement nappes is recorded by a continuum of retrograde high-T blueschist- and greenschist-facies mineral assemblages. The latter assemblages have been successfully dated by Rb–Sr geochronology on white micas at 38–36 Ma (Hunziker 1970, 1974; Hunziker et al. 1992; Inger and Ramsbotham 1997; Amato et al. 1999) for the Zermatt-Saas ophiolite and Penninic continental units, including the Monte Rosa and Gran Paradiso nappes. Continued cooling and final exhumation is constrained by the zircon fission-track ages noted above, as well as 24–14 Ma apatite fission-track ages (T_c = 60–120°C; Hurford and Hunziker 1989; Hurford et al. 1991; Bistacchi et al. 2001).

Monte Rosa nappe

The study area (Fig. 2) is located within the internal (southern) Monte Rosa nappe near the front of the Indren glacier, Gressoney Valley, Italy. In the 1980s, the area was still hidden by glacial cover, but recent retreat of the glacier terminus has exposed the outcrops studied here. Overall, the Monte Rosa nappe is composed of two main groups of pre-Alpine protoliths (Bearth 1952; Dal Piaz 1971, 1993, 2001; Dal Piaz and Lombardo 1986): a pre-granitic metamorphic complex, represented by high-grade (sillimanite + K-feldspar) paragneiss and cordierite-rich migmatites of Variscan or older age, and a large, Late Paleozoic pluton of granitic-granodioritic composition, often porphyritic and rich in aplitic-pegmatitic dikes. The granitoids intruded the surrounding paragneiss in the Late Carboniferous (Hunziker 1970; Frey et al. 1976; Engi et al. 2001a). Younger, Permian ages were obtained by U–Pb SHRIMP geochronology of zircons that are interpreted to reflect igneous ages (270 Ma), as well as monazite Th–Pb geochronology (268 ± 2 Ma) (Lange et al. 2000; Engi et al. 2001a; Pawlig et al. 2001). The Permian ages may correspond to a later magmatic event or to the Permian-Triassic lithospheric extension and related thermal perturbation that is extensively recorded in the western South-Alpine basement and some Alpine nappes (Lardeaux and Spalla 1991; Dal Piaz 1993). Sharp intrusive features are locally preserved (e.g., Castor-Lyskamm ridge) not far from the study area.

The response of the Monte Rosa nappe to Alpine metamorphism was dependent on lithology. In little deformed paragneisses and migmatites, the HP imprint is recorded by pseudomorphic replacement of sillimanite and cordierite by very fine aggregates of kyanite and kyanite + garnet, respectively. No sodic pyroxene has been found in massive metagranitoids, in marked contrast to the widespread occurrence of jadite in the Sesia-Lanzo zone to the south. In high strain Alpine domains, the HP imprint is recorded by: (1) garnet-phengite micaschists (±chloritoid or Na-amphibole) that were developed in pre-granitic paragneisses; (2) eclogitic boudins enclosed within garnet phengite micaschist; and (3) whiteschists, characterized by garnet, phengite, kyanite, Mg-chloritoid and talc, including white mica–rich mylonites, that were derived from metasomatized granitic rocks. The greenschist-facies overprint is sparsely to pervasively distributed and is characterized by albite-rich schists that contain new biotite, epidote, chlorite ± calcic amphiboles, as well as albite amphibolites that contain albite, calcic amphibole symplectites, epidote, chlorite, and titanite.

A pervasively deformed shear zone (Furgg zone) marked by trails of mafic boudins was recognized by Bearth (1952, 1958) along the Swiss northern margin of the Monte Rosa nappe; this zone lies in direct contact with the overlying Zermatt-Saas ophiolite. The matrix consists of heterogeneous metasediments and leucocratic rocks of presumed Permian-Mesozoic age. Mafic

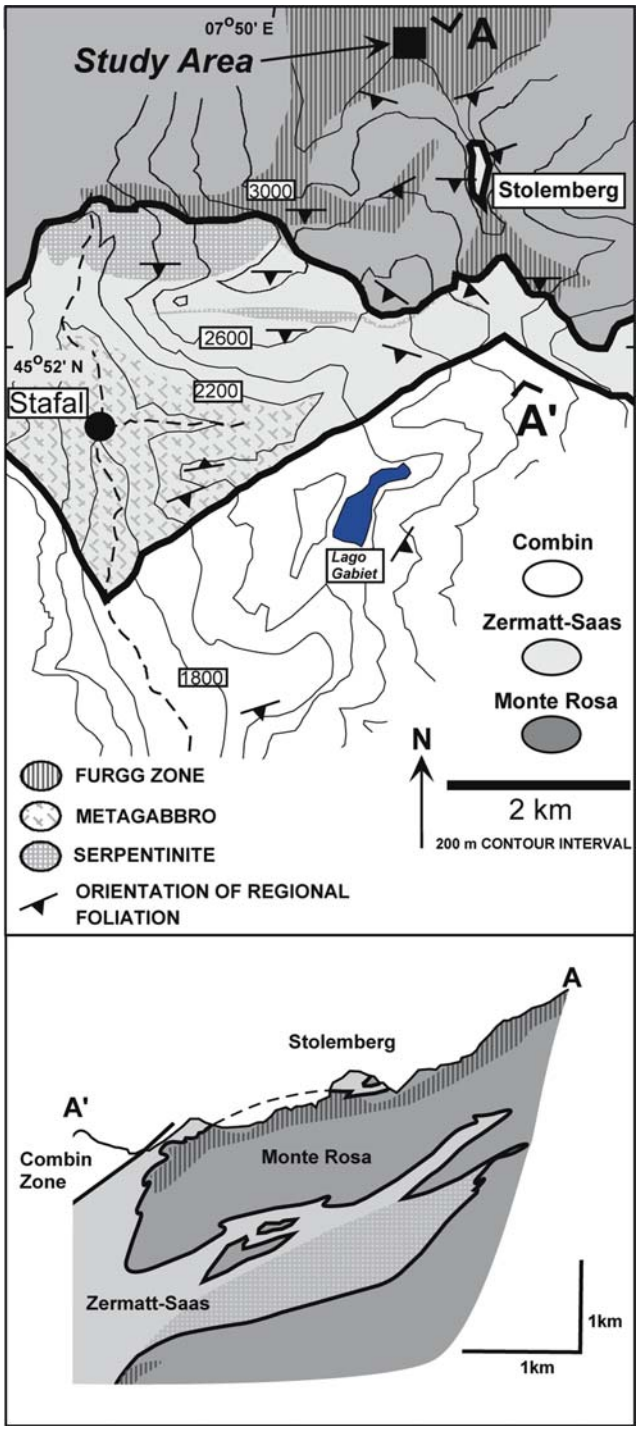

Fig. 2 Simplified geologic map and cross section (modified from Gosso et al. 1979) of the sample area at the head of Val di Gressoney, Italy (after Dal Piaz and Lombardo 1986; Bigi et al. 1990; Reddy et al. 1999). The sample location is within the Furgg Zone (Dal Piaz 2001). Foliation dip is variable and generally dips between 30 and 80°. Note the relatively planar contact between the Combin Zone and Zermatt-Saas ophiolite as opposed to the folded contact between the Zermatt-Saas ophiolite and Monte Rosa nappe (Gosso et al. 1979). Elevations are in meters. The *dashed line* represents major drainages in the area. *Bold lines* are tectonic contacts between units

boudin-rich zones also occur along the Italian southern side of the Monte Rosa massif, from the Ayas and Sesia valleys, through the Gressoney-Indren area (e.g., Dal Piaz 2001, and references therein). These boudins display Alpine age eclogite-facies mineral assemblages (Dal Piaz and Gatto 1963). Locally, some metabasaltic blocks contain intrusions of granitic material, confirming their pre-Mesozoic protolith age (Darbellay 2005). Similar boudins derived from pre-Variscan protoliths are documented by Liati et al. (2001) on the eastern side of the Monte Rosa massif.

This study focuses on HP metabasite and associated micaschists (formerly high-grade host rocks) that are situated well within the southern Furgg zone (Dal Piaz 2001). The metabasic rocks studied here are not likely to be tectonic slivers of the Zermatt-Saas ophiolite complex, but are primary components of the crystalline basement of the Monte Rosa nappe. The chemistry of the eclogitic boudins sampled within the study area by Ferrando (2002) indicate that these are continental tholeiitic basalts and are significantly different in composition from metabasite of the Zermatt-Saas ophiolite (Beccaluva et al. 1984) and other Mesozoic ophiolitic suites associated with the Piedmont-Ligurian Ocean crust. A pre-Mesozoic origin of these rocks is supported by the presence of micro-inclusions of hornblende, rutile, and minor plagioclase inside the core of eclogitic garnet, indicating that these mafic bodies experienced amphibolite-facies (P = 0.5–0.7 GPa, T = 600°C) metamorphism prior to late Paleozoic intrusion of the Monte Rosa granite.

The general structural features of the southern Furgg Zone inside the southern Monte Rosa nappe are shown in Fig. 2. The tectonic contact between the Monte Rosa nappe and the overlying Zermatt-Saas ophiolite is deformed by a series of ENE-trending recumbent backfolds, whereas the basal thrust of the overlying blueschist facies Combin unit is flat (Fig. 2; Gosso et al. 1979). The eclogite boudins are enclosed in a generally E–W-striking, S-dipping foliation (S1, or earliest recognized foliation) defined by aligned minerals and compositional layering within the surrounding schist and gneiss. This foliation contains isoclinally folded eclogite (described below, Fig. 3) and, perhaps, isoclinal folds of primary lithologic layering (F1). Locally, the hinges of some isoclinal folds are defined by S1, indicating two generations of eclogite-facies isoclinal folds (e.g., F1a-b defined by Gosso et al. 1979). Boudinage (Fig. 3) of the eclogite-facies metabasite occurred during F1a and/or F1b development and was coeval with emplacement of the quartz–carbonate–white mica–rutile veins that occur in the boudin necks

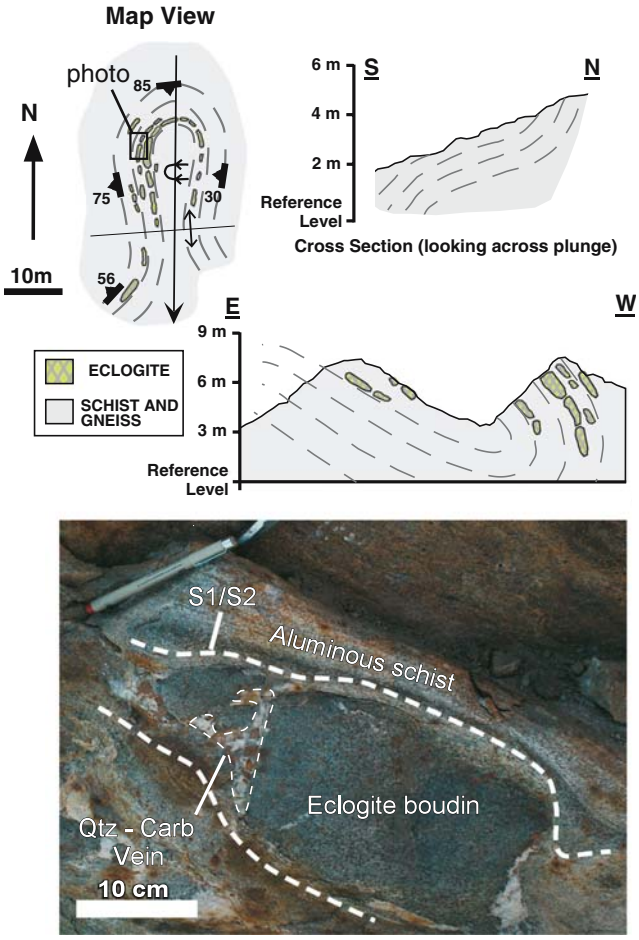

Fig. 3 Field sketch map and cross-sections of the sample area and photograph of an eclogite boudin. Metabasite boudins represent the type A eclogites discussed in the text. *Dashed lines* represent the trace of the S1/S2 foliation (see text). Note how the foliation wraps the eclogite boudins (neck folds) and the occurrence of quartz–carbonate material within its neck. Reference levels are arbitrarily set to 0 m. The overturned synform shown in the map view represents the geometry of the F3 fold observed in the sample area. See the text for a more detailed explanation

and in tension cracks. Subsequent deformation locally formed tight, N–S trending, overturned (F2) folds (Fig. 3); it is unknown if these folds are the result of E–W directed shortening, considered unlikely, or are partially eroded sheath-type folds. Broad, open E–W trending folds appear to deform the F2 fold axes in the study area.

Lithologic descriptions

The study area is characterized by thin eclogitic beds and small boudins that occur within aluminous schists. Veins of quartz–carbonate–white mica–rutile are

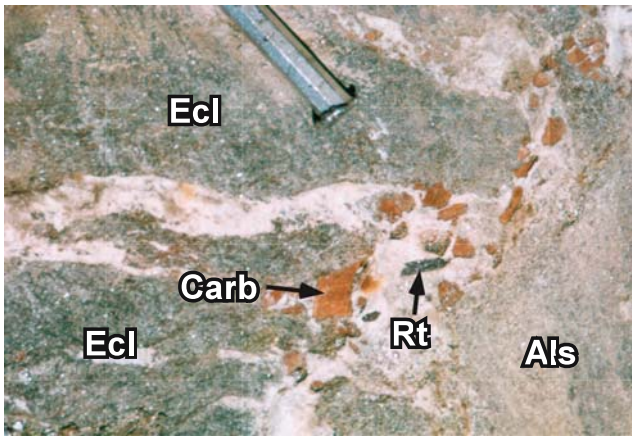

Fig. 4 Photograph of the type A eclogite-vein-schist and gneiss field relations. The chisel in the upper part of the photo is 3.5 cm in diameter. Note the large rutile (*Rt*) within a matrix of quartz–carbonate (*Carb*)–white mica. The veins commonly wrap the eclogite (*Ecl*) boundings and locally completely enclose them. Eclogite was adjacent to the aluminous schist (*Als*) at the time of vein emplacement

commonly present along the contacts between eclogite and schist and as veins within fractured eclogite boudins (Figs. 3, 4).

Eclogite

Mineral chemistry data and petrologic estimates of the peak Alpine HP imprint are $P \geq 1.3$ GPa and $T = 535$–620°C as marked by the eclogite-facies assemblage (garnet, omphacite, rutile, paragonite, and phengite). The decompressional (exhumation) P–T conditions are recorded by Ca–Na amphiboles and albite-actinolite symplectites (Dal Piaz and Lombardo 1986; Ferrando 2002; Ferrando et al. 2002). This metamorphic evolution is very similar to that recorded in the overlying Zermatt-Saas ophiolite.

Eclogite in the study area occurs as two main types, defined here as types A and B, based on mineralogy, mineral texture, and field occurrence. The type A eclogites are generally decimeter to several meters in size, lozenge-shaped boudins that have aspect ratios sometimes in excess of 10:1. They are commonly associated with quartz–carbonate–white mica–rutile veins, which tend to be oriented at high angles to the long axis of the boudins. Locally, type A eclogites show evidence of brecciation associated with emplacement of the veins. The mineralogy of the type A eclogites (Fig. 5a) consists of equidimensional garnet + omphacite + Na-amphibole + paragonite + rutile ± quartz ± clinozoisite ± sulfides, and the mineral assemblage, with the exception of rutile, mica, and sulfides, is roughly equigranular. Garnet, omphacite, Na-amphibole,

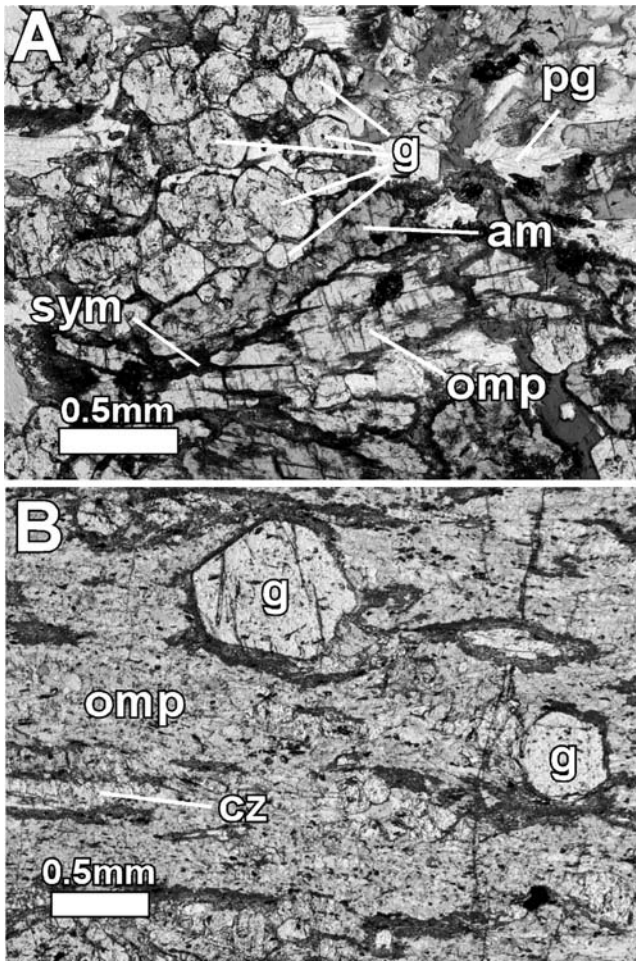

Fig. 5 Photomicrographs of types A and B eclogites. **a** Type A eclogite. This group of eclogites typically display an equigranular texture. Note the large grain of omphacite (*omp*) with surrounding amphibole-albite symplectite (*sym*). Garnets (*g*) are subhedral and generally occur in clusters of several grains. Na-amphibole (*am*) appears to be in textural equilibrium with garnet and omphacite. Paragonite (*pg*) is uncommon, but occurs as large stubby flakes. All minerals are randomly oriented in type A eclogites. **b** Type B eclogite. This group of eclogite is typically finer grained than type A eclogites and they display a porphyroblastic texture. Garnet (*g*) is typically idioblastic and occurs in a matrix of fine-grained, well-aligned omphacite (*omp*). Paragonite is commonly aligned in the foliation. Clinozoisite (*cz*) occurs aligned in the foliation and also as grains that grow across the foliation

and white mica are all generally sub-equal in abundance. Garnets are typically very fresh, subidioblastic, 0.25–2 mm in diameter, and often occur in clusters. Omphacite occurs as blocky crystals that typically are randomly oriented but are in textural equilibrium with garnet. Retrograde textures involving breakdown of omphacite to Ca–Na amphibole-rich symplectite is variably developed; most metabasite boudins contain only albite-amphibole symplectite (after cpx), whereas others contain only minor retrogression of primary omphacite. The other phases constituting the eclogite-facies mineral assemblage appear to be in textural equilibrium with garnet and omphacite and contain little evidence of retrogression to greenschist-facies mineral assemblages in the samples studied here.

The type B eclogites generally occur as relatively thin (5–50 cm), tabular layers within the micaschist of the Monte Rosa nappe. The eclogite contains a well-developed foliation that is defined by layering and aligned eclogite-facies minerals. Locally, the eclogitic foliation (S1) is isoclinally folded with axial planes parallel to the regional foliation (S2) in the host rocks. Unlike the type A eclogites, the type B eclogites are not associated with quartz–carbonate–white mica–rutile veins. The mineralogy of the type B eclogites (Fig. 5b) consists of garnet + omphacite + white mica + clinozoisite + rutile ± sulfides, where omphacite is the most abundant phase (>60–70% by volume). Garnets are idioblastic, 0.1–1 mm in diameter, and are generally surrounded by a matrix of fine-grained (<0.2 mm diameter), sub-equant to elongate, well-aligned omphacite. Clinozoisite grains are prismatic to stubby and locally grow across the foliation defined by omphacite, white mica, and trains of sulfide minerals. Where clinozoisite has grown across the foliation, trains of sulfide minerals define an internal foliation that is parallel to that defined by omphacite. Overall, retrograde greenschist-facies assemblages are sparse in these lithologies. Where present, retrograde assemblages are associated with thin shear zones that initiated either during formation of eclogitic mylonite or retrogression and contain amphiboles that are zoned from blue amphibole cores to green amphibole rims, calcic amphiboles + albite, titanite, and calcite. A thorough treatment of the types A and B eclogites is beyond the scope of this article but is the focus of another manuscript (Lapen et al., in preparation).

Quartz–carbonate–white mica–rutile veins

The quartz–carbonate–white mica–rutile veins are typically associated with the type A eclogites. The veins are usually composed of very large (1–5 cm in diameter) iron carbonate crystals surrounded by a finer-grained aggregate of quartz and white mica (±chlorite and Ca–Na amphibole), as well as sparse to abundant rutile (Fig. 4). Rutile occurs as two textural types: (1) relatively small, acicular grains (>2 cm long by <0.5 cm wide) that are commonly contained within carbonate and quartz, and (2) large, stubby grains (1–2 cm by 1–2 cm) that are exclusively contained within the quartz + white mica matrix of the vein. Rutiles from both textural types are identical with respect to

major element compositions (Table 1), but, as will be shown below, they are different with respect to their initial Pb isotope compositions. All rutiles contain very small (<1 μm) lamellae of exsolved ilmenite as well as variable amounts of ilmenite surrounding the rutile grains (Fig. 6). Retrograde assemblages in the veins consist of chlorite after carbonate, blocky to amoeboid-shaped poikiloblastic albite, and aggregates of titanite that presumably are a reaction product of rutile + carbonate + quartz that formed during decompression, cooling, and/or changes in X_{CO2}.

Schist

Mica–rich schists are interlayered with more quartz- and feldspar-rich rocks at the scale of several meters to decimeters. Both the aluminous and quartzofeldspathic schists are well foliated and host the types A and B eclogites. The mineralogy of the aluminous schist of the Monte Rosa nappe has been described by Bearth (1952), Dal Piaz (1971), and Dal Piaz and Lombardo (1986). The degree to which the Alpine HP mineral assemblages overprint the earlier assemblages and in turn are overprinted by the greenschist-facies tectonic and metamorphic reworking is typically a function of the amount of strain partitioning during polyphase Alpine metamorphism (Gosso et al. 1979; Dal Piaz and Lombardo 1986, and references therein). A typical mineral assemblage in high-strain schists that are not strongly retrogressed is phengite, garnet, chloritoid, kyanite, rutile, quartz, ±carbonate, ±Na-amphibole (Dal Piaz 1971; Dal Piaz and Lombardo 1986).

Textural relations between eclogite, schist, and quartz + carbonate + white mica + rutile veins

The quartz–carbonate–white mica–rutile veins are primarily associated with metabasaltic boudins and are generally exposed as tension veins within metabasite and as veins along the contact between metabasite and the schist. One very fresh eclogite (sample TL-03-99) has abundant tension veins as well as very coarse-grained veins that surround the eclogite. Because the veins contain abundant hydrous phases and mineralogical/textural features that indicate high volatile contents, it is expected that they would facilitate recrystallization if emplacement of the veins occurred at *P–T* conditions that differed significantly from the eclogite-facies assemblage in the mafic boudins. Photographs and photomicrographs of the eclogite/vein contact (Fig. 7) indicate no correlation in the degree of post-eclogite retrogression, as evidenced by symplectite development around omphacite, with proximity to either the tension or surrounding veins. We also note that inclusions of sub-idioblastic garnet, Na-amphibole, as well as displaced fragments of garnet + omphacite + paragonite occur within the veins, indicating that they were not emplaced prior to or after the onset of

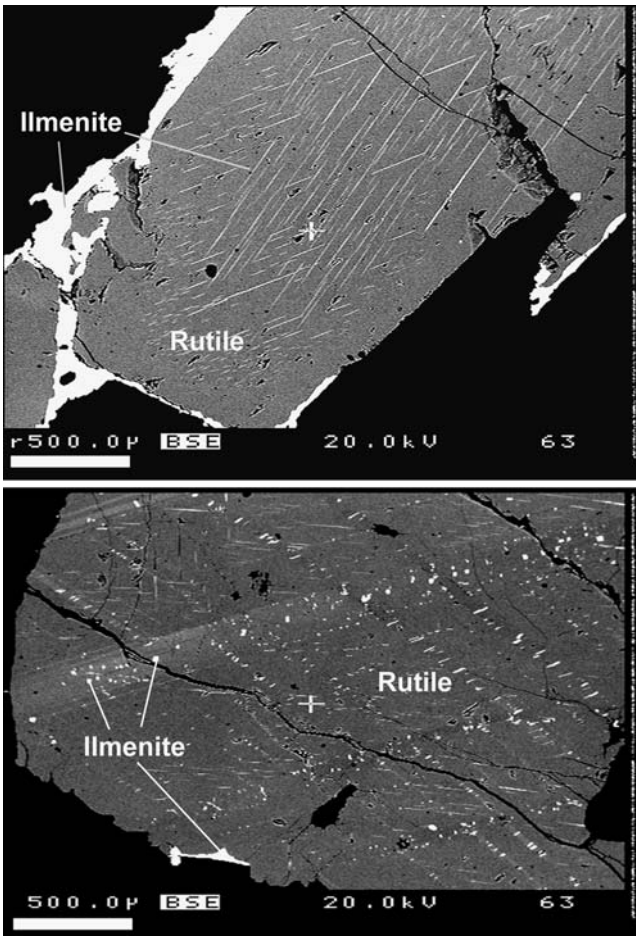

Fig. 6 Backscatter electron image (*BSE*) of representative rutiles. The *bright areas* represent ilmenite whereas the *gray* regions represent rutile. The fine ilmenite within both rutile images represent crystals exsolved during cooling after peak metamorphic conditions. The amount and orientation of lamellae corresponds to differences in crystallographic orientation within the grain, which also results in variable electron backscattering properties in the plane of the section

Table 1 Major element compositions of rutile from all samples analyzed for U–Pb and oxygen isotopes

TiO_2	98.88 ± 0.39
Cr_2O_3	0.084 ± 0.62
$V2O_3$	0.171 ± 0.08
FeO	0.503 ± 0.159
Total	99.81 ± 0.39

Data is in wt. %, number of analyses = 42, the scatter (±*xx* refers to the 2-SD total variation between samples)

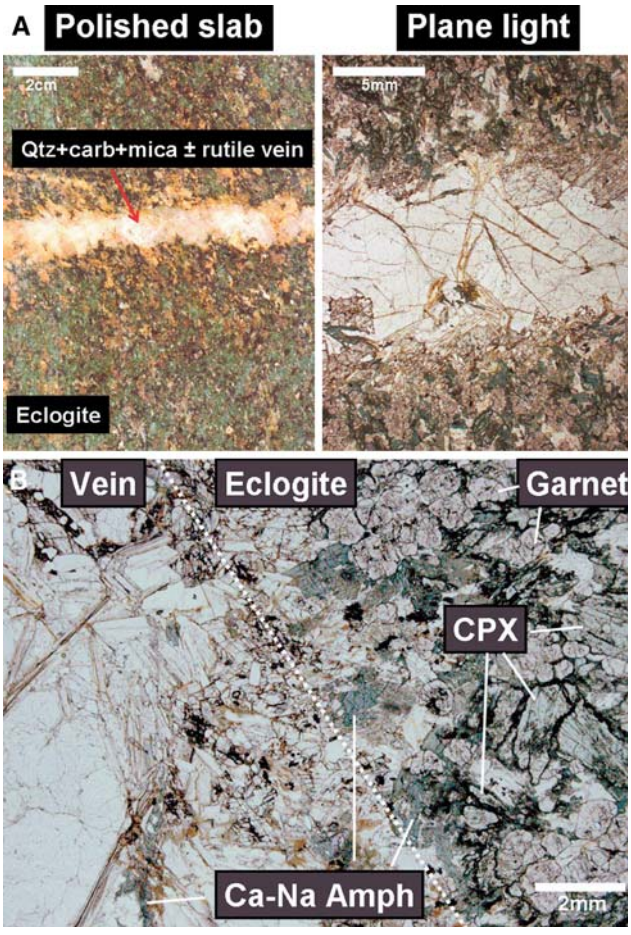

Fig. 7 Photographs of eclogite Sample TL-03-99 and tension vein. **a** A polished slab of eclogite as well as a photomicrograph in plane light of the same area. Note the lack of any retrogression of the eclogite-facies minerals associated with the vein. **b** Photomicrograph of the vein-eclogite contact. Note that omphacite (*cpx*) and garnet are stable phases adjacent to the veins suggesting that the veins intruded at eclogite facies conditions. Locally, garnet and Na-amphibole occur as inclusions in the veins, indicating that the veining post-dates formation of some HP minerals and that the veins and eclogite did not share a prograde evolution

eclogite-facies metamorphic conditions. We conclude that the veins are in textural equilibrium with their surrounding eclogite-facies mineral assemblages. The veins, therefore, must have been emplaced into the eclogite and surrounding crystalline basement during Alpine eclogite-facies metamorphism.

Analytical methods

Approximately 10–80 mg of rutile was removed from the vein material by sawing the sample into chips and then extracting the rutile physically by breaking it free from the matrix. The rutile was broken into ~1 mm diameter fragments, which were then hand picked with a binocular microscope for purity. The picked mineral separates were leached for ~15 min in cold 2 M doubly-distilled HF, followed by a leaching step in warm, distilled 6 M HCl for 45–60 min in an effort to remove all surficial contamination. Following acid cleaning, the samples were washed in an ultrasonic bath of twice-distilled H_2O. The rutile samples were placed into small Teflon^{TM} capsules with 0.3 ml twice-distilled 29 M HF and 0.05 ml 14 M HNO_3. The samples were then spiked with a mixed ^{205}Pb–^{235}U isotope tracer that was cross-calibrated against the 'MIT mixed U–Pb gravimetric solution' available from EARTHTIME^{TM} for interlaboratory cross-calibrations. Based on comparisons against the EARTHTIME gravimetric solution, we measured a molar U/Pb ratio of 68.43 ± 0.26% (2σ, $n = 3$), which differed by ~1% from our previous calibration that was based on gravimetric solutions prepared at U.W. Madison. The ages presented in this paper are based on the latest calibration. The Teflon capsules were placed into a single large Parr^{TM} bomb that contained 8 ml of 29 M HF and heated to 200°C for 24–30 h. The samples were dried on a hotplate and 1 ml of a 6 M HCl–0.2 M HF solution was added to the samples, followed by a second dry down to ensure spike-sample equilibration. The samples were loaded onto 1 ml of Dowex AG1X8 anion exchange resin in a mixture of 0.6 M HBr–0.2 M HF, and U (and other matrix elements) was eluted with 0.6 M HBr; Pb was eluted with 6 M HCl. Subsequent chemical purification of Pb was achieved using the same chemical procedure described above, applied to a 0.3 ml volume of anion exchange resin. Uranium was purified using anion exchange resin in HNO_3. Total Pb and U blanks were <20 and <10 pg, respectively.

Approximately 5–50 mg of carbonate and matrix quartz + mica were taken from the material remaining from the rutile extraction procedure and crushed to 1–0.5 mm diameter fragments. The samples were picked for purity with a binocular microscope, leached for 1 h in cold 1 M HCl, and then washed with twice-distilled H_2O for 3 h in an ultrasonic bath. The carbonate samples were dissolved in 3 ml distilled hot 6 M HCl; the quartz + mica fraction was dissolved in 3 ml distilled 29 M HF–1 M HNO_3. After drying, ~2 ml of 6 M HCl was added to each sample and then the samples were dried again. This process was repeated until there were no remaining precipitates as detected by centrifuging in 2 ml of 6 M HCl. The samples were split into two equal fractions by volume, where one fraction was spiked with a ^{206}Pb–^{208}Pb–^{235}U mixed double spike and the other split was not spiked, as required by standard 'double spike' methods. Pb and U were

separated with anion exchange resin in HBr and HNO_3, respectively.

Isotope ratio measurements were performed on the U.W. Madison GV Instruments *Sector 54* and GV Instruments *IsoProbe* mass spectrometers for Pb and U, respectively. Lead isotope ratios for rutile samples were measured on a single collector Daly detector; Pb isotope ratios for carbonate and matrix quartz + mica were measured in static mode on Faraday collectors. Instrumental mass fractionation was monitored for rutile samples by analysis of NBS-981 and 982, which yielded an average mass bias of +0.14 ± 0.05%/amu (2σ, $n = 7$) that was applied to the measured data. To increase the precision of the Pb isotope ratio measurements of carbonate and matrix quartz + mica samples, measured ratios were corrected for instrumental mass fractionation using a ^{206}Pb–^{208}Pb double spike and the algorithms in Johnson and Beard (1999). Instrumental mass fractionation during U analyses was corrected based on measurement of natural U standards that were interspersed with the samples, which yielded an average mass bias of +0.30 ± 0.03%/amu (2σ, $n = 35$).

Mineral separates of quartz and rutile for oxygen isotope analyses were removed from the samples used for U–Pb analyses by the same methods described above. Quartz and rutile were selected from grains that were in contact with each other to ensure the best chances for isotopic equilibrium between the analyzed phases. Once removed from the samples, the grains were washed in warm 1 M HCl for 15–20 min to remove carbonate and then rinsed in distilled H_2O for 5 min. One to 3 mg samples of quartz and rutile were fluorinated in a Pt sample holder as coarse sand using a CO_2-laser and F_2 as the reagent. The O_2-gas was directly measured on a Finnigan *MAT 253* mass spectrometer at the University of Lausanne; analytical techniques were similar to those reported in Sharp (1992). All O isotope analyses were duplicated, yielding an average precision of ±0.2‰ (1σ) and all values listed in Table 2 are reported in standard per mil notation relative to V-SMOW. Twelve analyses of the in-house Lausanne-1 quartz standard (normalized to $\delta^{18}O = 9.6‰$ for NBS-28) were performed during the 6 days of sample analyses and yielded an average value of $\delta^{18}O = 18.09 \pm 0.19‰$ (1σ, $n = 12$).

Mineral compositions were determined with a Cameca SX-51 electron microprobe at U.W. Madison using an accelerating voltage of 15 kV, a beam current of 20 nA, and a suite of analyzed natural and synthetic standards. A $\varphi(\rho z)$ data reduction program was used to correct the data (Armstrong 1988).

Results

Eight rutile and seven carbonate and quartz + white mica mineral fractions from five samples of the quartz–carbonate–white mica–rutile veins associated with the

Table 2 Oxygen isotope data for quartz and rutile from quartz–carbonate–white mica–rutile veins

Sample	$d^{18}O$ qtz	$d^{18}O$ ru		$d^{18}O$ qtz	$d^{18}O$ ru	D qtz-ru	T (°C)
TL-02-45(1)	9.81						
TL-02-45(1)	9.78	1.03	Mean	9.76	0.90	8.87	461
TL-02-45(1)	9.69	0.76	SD	0.06	0.19	0.20	8
TL-02-45(2)	9.55	0.76	Mean	9.59	0.62	8.98	457
TL-02-45(2)	9.63	0.47	SD	0.06	0.21	0.21	9
TL-03-96(1)	9.89	2.79					
TL-03-96(1)	9.86	2.66	Mean	9.63	2.54	7.09	548
TL-03-96(1)	9.12	2.15	SD	0.44	0.34	0.55	34
TL-03-96(2)	9.73	3.01	Mean	9.73	2.87	6.86	562
TL-03-96(2)		2.73	SD		0.20	0.20	12
TL-04-120A(1)	9.38	1.34	Mean	9.22	1.29	7.94	503
TL-04-120A(1)	9.06	1.23	SD	0.23	0.08	0.24	12
TL-04-120A(2)	9.85	1.14					
TL-04-120A(2)	9.76	1.41	Mean	9.70	1.24	8.46	479
TL-04-120A(2)	9.50	1.18	SD	0.18	0.15	0.23	11
TL-04-123(1)	9.48	0.05					
TL-04-123(1)	9.50	0.30	Mean	9.45	0.16	9.28	445
TL-04-123(1)	9.36	0.14	SD	0.08	0.13	0.15	6
TL-04-126(1)	10.62	2.89	Mean	10.37	2.51	7.86	507
TL-04-126(1)	10.11	2.13	SD	0.36	0.54	0.65	34

Uncertainties from replicate analyses are at 1σ (SD) precision. Numbers in parentheses represent different mineral domains from the same sample. All data has been normalized to $\delta^{18}O = 9.6‰$ for NBS-28; all data are presented relative to V-SMOW. Temperatures are calculated with the quartz–rutile fractionation factor of Agrinier (1991)

Qtz quartz, *Ru* rutile

type A eclogite boudins were analyzed for U and Pb contents and isotope compositions. Oxygen isotope measurements on rutile and quartz from the same samples constrain the temperatures at which the veins were emplaced. In addition, pressure and temperature estimates of the eclogite boudins based on mineral compositions place additional constraints on the *P–T* conditions.

U–Pb age and isotope data

Rutiles from within a single quartz–carbonate–white mica–rutile sample and from samples separated by several meters have sufficient spread in U/Pb ratios to yield very precise age determinations (Table 3). The small rutile crystal group yielded a ^{238}U–^{206}Pb isochron age of 42.24 ± 0.49 Ma (2σ, MSWD = 0.38, n = 4) and rutile from the large crystal group yielded a ^{238}U–^{206}Pb isochron age of 42.88 ± 0.34 Ma (2σ, MSWD = 1.5, n = 4; Fig. 8a). A ^{235}U–^{207}Pb isochron age of 40.4 ± 2.2 Ma (2σ, MSWD = 4.0, n = 8; Fig. 8b) was determined by plotting all rutiles from both textural types and indicates that both the ^{238}U–^{206}Pb and ^{235}U–^{207}Pb ages are concordant within error. The weighted average of all ^{238}U–^{206}Pb ages is 42.64 ± 0.55 (2σ). All ages and uncertainties were calculated using IsoPlot v.2.49 (Ludwig 2001) and error propagation equations of Ludwig (1980).

Although both rutile textural types yield the same ages, their initial $^{206}Pb/^{204}Pb$ ratios are significantly different. Moreover, differences in initial $^{206}Pb/^{204}Pb$ are also observed with the vein carbonate and matrix quartz + white mica. Initial $^{206}Pb/^{204}Pb$ ratios for the texturally small rutile group was $^{206}Pb/^{204}Pb$ = 17.68 ± 0.10 (2σ), whereas the large rutiles had an initial $^{206}Pb/^{204}Pb$ = 18.41 ± 0.12 (2σ). The matrix fraction of quartz + white mica and iron carbonate had very low U/Pb ratios and the highest initial $^{206}Pb/^{204}Pb$ ratios at 18.97 ± 0.01 (2σ). The Pb in the matrix quartz + white mica and iron carbonate was not in isotopic equilibrium with the rutile, thus precluding the use of the matrix quartz + white mica and iron carbonate in the U–Pb isochrons or as an indicator of the initial Pb isotope composition of the rutiles.

Oxygen isotope thermometry of quartz and rutile

$^{18}O/^{16}O$ ratios were measured for eight quartz–rutile pairs in five samples (Table 2). In most cases, the mineral samples were collected from areas of the veins that contained primarily quartz and rutile (and some mica). $\delta^{18}O$ values for rutile are highly variable between the five samples (+0.05 to +3.0‰), whereas quartz had relatively homogenous $\delta^{18}O$ values of +9.0 to +10.9‰; this may reflect the fact that rutile is a minor repository for O in the veins and hence should

Table 3 Uranium and lead concentrations and lead isotopic compositions for rutile, carbonate, and matrix quartz + mica from veins within the Monte Rosa massif and associated eclogite boudins

Lab number	Sample number	Material	ppm U	ppm Pb[b]	$^{238}U/^{204}Pb$[a]	$^{206}Pb/^{204}Pb$[a]	±[c]	$^{235}U/^{204}Pb$[a]	$^{207}Pb/^{204}Pb$[a]	±[c]
4P-548	TL-02-96	Rutile (sm)	5.401	0.164	2,182	32.091	0.687	15.44	16.107	0.258
5P-34	TL-02-45	Rutile (sm)	1.744	0.065	1,676	28.662	0.353	12.15	16.014	0.307
5P-36	TL-02-45	Rutile (sm)	0.918	0.145	347.4	19.970	0.410	2.520	15.551	0.285
5P-37	TL-02-96	Rutile (sm)	2.170	0.070	1,961	30.595	0.422	14.22	15.976	0.605
5P-39	TL-02-120A	Rutile (lg)	3.228	0.041	7,073	65.581	0.301	51.30	17.650	0.217
5P-40	TL-02-120A	Rutile (lg)	3.124	0.108	1,860	30.859	0.160	13.49	16.076	0.191
5P-41	TL-02-123	Rutile (lg)	1.166	0.009	19,089	144.40	2.52	138.4	20.967	1.124
5P-42	TL-02-126	Rutile (lg)	1.277	0.068	1,133	25.897	0.427	8.216	15.753	0.497
4P-301	TL-03-96	Carbonate	0.128	135.903	0.0517	18.9716	0.0036	0.0004	15.6757	0.0029
4P-303	TL-03-96	Carbonate	0.121	27.550	0.2414	18.9612	0.0038	0.0018	15.6688	0.0031
5P-73	TL-02-45	Matrix	1.393	20.249	3.865	19.1248	0.0038	0.0280	15.6780	0.0030
5P-74	TL-03-96	Carbonate	0.034	35.938	0.0524	19.0081	0.0037	0.0004	15.6514	0.0031
5P-75	TL-04-120A	Carbonate	0.202	34.849	0.3242	18.9843	0.0038	0.0024	15.6679	0.0031
5P-76	TL-04-123	Matrix	0.746	1.516	27.75	19.2339	0.0039	0.2012	15.6830	0.0030
5P-77	TL-04-126	Carbonate	0.011	4.613	0.1351	18.9740	0.0036	0.0010	15.6656	0.0031

(sm) and (lg) refer to the small and large size groups of the rutiles, respectively (see text for details). Errors for the $^{235}U/^{204}Pb$ and $^{238}U/^{204}Pb$ are ±0.5%

[a] Corrected for blank and instrumental mass fractionation

[b] Pb concentration less blank

[c] Errors are based on the error propagation equations of Ludwig (1980)

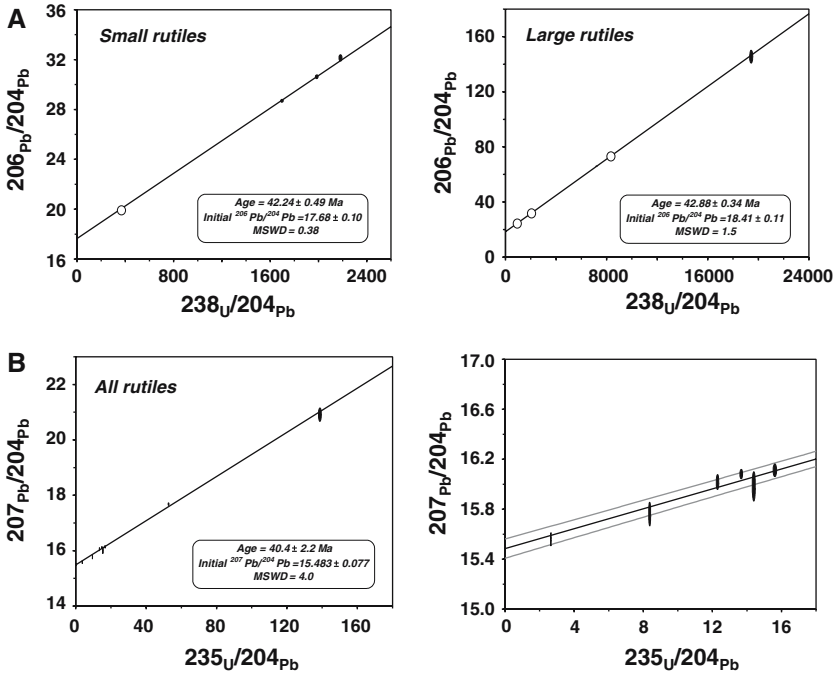

Fig. 8 U–Pb isochron diagrams for rutiles. All age and initial isotope data are shown at the 2σ level of uncertainty. **a** ^{238}U–^{206}Pb isochron diagrams for the texturally small grains (*left*) and texturally large grains (*right*). Because of the large spread in isotope composition, some data points are difficult to see. These are labeled with an open circle for clarity. **b** ^{235}U–^{207}Pb isochron diagram for all eight rutile samples (both the large and small grains; see text for details). The figure on the right represents a detail of the low $^{235}U/^{204}Pb$ region with a 2σ error envelope (*light gray lines*)

have the greatest variability in $\delta^{18}O$ values if changes in temperature occurred during vein formation. Alternatively, the rutiles could be zoned in their oxygen isotope compositions (i.e., growth zoning) or have been altered during ilmenite exsolution. The variability in $\delta^{18}O$ of rutile does not correlate to its initial Pb isotope composition or U/Pb ratios, nor are these correlated to variations in mineral chemistry or proportion of exsolved ilmenite. This raises the possibility that the host quartz may have exchanged with fluids after quartz–rutile equilibration and resulted in relatively homogeneous $\delta^{18}O$ values for quartz but variable quartz–rutile fractionations.

The quartz–rutile $^{18}O/^{16}O$ fractionations for all samples range from +6.86 to +9.28‰, with a weighted average of +8.48 ± 0.38‰ (1σ, $n = 8$). These fractionations produce oxygen isotope temperatures of 445–560°C (Table 2) using the calibration of Agrinier (1991), and 460–580°C using the calibration of Matthews (1994). The oxygen isotope temperatures calculated using the weighted average quartz–rutile fractionation are 491 ± 36°C (2σ) and 472 ± 35°C (2σ) using the Agrinier (1991) and Matthews (1994) calibrations, respectively. Although there may be uncertainties regarding isotopic equilibrium between quartz and rutile, oxygen isotope thermometry yields temperatures that overlap those estimated on Fe–Mg exchange between garnet and omphacite in the host eclogites at this locality (Dal Piaz and Lombardo 1986; Ferrando 2002; this study, below).

Mineral chemistry and pressure and temperature data of type A eclogites

Compositions of coexisting garnet and pyroxene from an extremely fresh type A eclogite (TL-03-99) were determined by electron microprobe (Table 4). Several mineral analyses were performed in four domains within two thin sections that also contain coexisting vein material. Each grain was inspected with transmitted light and back-scattered electrons for lack of inclusions and homogeneity prior to electron microprobe analysis.

The garnet rim compositions are typically almandine (65%), grossular (21%), pyrope (13%), and spessertine (1%), whereas garnet cores contain higher proportions of spessertine (>4%) and almandine (68%) and less pyrope (<7%), consistent with prograde element zoning in garnet (e.g., Ghent 1988). The average composition of clinopyroxenes, where Fe^{3+} was calculated by methods outlined in Droop (1987), are jadeite (47.5%), diopside (30%), acmite (9.5%), and hedenbergite (13%); these compositions are typically constant from core to rim within individual crystals, as well as crystals throughout sample TL-03-99.

Temperatures and minimum pressures were calculated for each of the four domains using the mineral compositions listed in Table 4 and from calibrations of the following equilibria:

Pyrope + three Diopside = Almandine + three Hedenbergite (Ravna 2000),

Jadeite + Quartz = Albite (Gasparik 1985).

Table 4 Mineral compositions used for thermobarometric calculations representing an average of >5 mineral analyses per domain

	Domain A		Domain B		Domain C		Domain D	
	Garnet	Pyroxene	Garnet	Pyroxene	Garnet	Pyroxene	Garnet	Pyroxene
SiO_2	37.60	55.85	37.77	55.46	37.64	55.46	37.67	55.73
TiO_2	0.05	0.02	0.05	0.06	0.03	0.08	0.03	0.06
Al_2O_3	21.09	11.52	21.32	10.48	21.49	10.07	21.38	9.83
Fe_2O_3	–	3.91	–	3.24	–	3.45	–	3.37
FeO	29.52	4.52	28.73	4.94	28.70	5.22	29.05	4.94
MnO	0.70	0.03	0.47	0.05	0.41	0.01	0.56	0.04
MgO	2.50	5.07	3.75	5.76	3.37	5.82	3.11	6.27
CaO	8.00	9.60	7.57	10.96	7.46	11.05	7.66	11.69
Na_2O	–	8.83	–	8.00	–	7.90	–	7.67
Sum	99.47	99.35	99.66	98.94	99.11	99.07	99.47	99.60
Si	3.00	2.01	2.99	2.01	3.00	2.01	3.00	2.01
Ti	0.00	0.00	0.00	0.00	0.00	0.00	0.00	0.00
Al	1.99	0.49	1.99	0.45	2.02	0.43	2.00	0.42
Fe^{3+}	–	0.11	–	0.09	–	0.09	–	0.09
Fe^{2+}	1.97	0.14	1.90	0.15	1.91	0.16	1.93	0.15
Mn	0.05	0.00	0.03	0.00	0.03	0.00	0.04	0.00
Mg	0.30	0.27	0.44	0.31	0.40	0.32	0.37	0.34
Ca	0.69	0.37	0.64	0.43	0.64	0.43	0.65	0.45
Na	–	0.62	–	0.56	–	0.56	–	0.54
Sum	8.00	4.00	8.01	4.00	7.99	4.00	8.00	4.00
% Alm	65.7		63.0		64.2		64.6	
% Sps	1.6		1.0		0.9		1.3	
% Prp	9.9		14.7		13.4		12.3	
% Grs	22.8		21.3		21.4		21.8	
	% Acm	10.5		8.8		9.4		9.1
	% Jd	51.2		47.5		46.3		44.7
	% Di	25.2		29.4		29.5		32.1
	% Hd	12.7		14.2		14.8		14.1
P (minimum, GPa):		1.16		1.35		1.32		1.21
	T (°C):	482		577		564		517

The letters represent individual domains within the very fresh sample TL-03-99. All garnet compositions shown here are from the mineral rims. Fe^{2+} and Fe^{3+} were determined with the method outlined in Droop (1987). Cr and K were below detection limits of the EMP. *P–T* data from calibrations of Ravna (2000) and Gasparik (1985)

Because stable albite is absent from the peak metamorphic eclogite-facies mineral assemblage, the calculated pressures are only a minimum estimate. The results (Table 4) are T = 480–570°C and P > 1.3 GPa, which are identical to *P–T* estimates of the Monte Rosa nappe by Dal Piaz and Lombardo (1986), Borghi et al. (1996), and Engi et al. (2001a). Similar *P–T* estimates of P > 1.3 and <2.0 GPa; T = 535–620°C were obtained from the same sample locality by Ferrando (2002) and Ferrando et al. (2002). Higher-pressure metamorphic conditions of 1.6 and 2.5 GPa (Chopin and Monié 1984 and Le Bayon et al. 2000, respectively) have been reported in chloritoid-bearing whiteschists to the west of the study area, possibly recording the peak pressure of the Monte Rosa nappe.

Discussion

Based on the textural relations between the quartz–carbonate–white mica–rutile veins and the eclogite-facies minerals in the metabasalt boudins, as well as the general agreement in temperature estimates by both quartz–rutile oxygen isotope thermometry of veins and garnet omphacite Fe–Mg exchange geothermometry of eclogite, we conclude that the veins were emplaced into the eclogite and surrounding schist at eclogite-facies conditions. The 42.6 ± 0.6 Ma U–Pb age of rutiles from the quartz–carbonate–white mica–rutile veins, therefore, firmly establishes a time point within the eclogite-facies metamorphic history of the Monte Rosa nappe, but not its duration. Our U–Pb ages are identical within error of the 43.0 ± 0.5 Ma Rb–Sr age of eclogite-facies metamorphism in the Gran Paradiso nappe (Meffan-Main et al. 2004). Based on their virtually identical metamorphic ages, alpine *P–T* history (Dal Piaz and Lombardo 1986; Borghi et al. 1996), and structural positions in the Alps, our data further strengthens previously proposed models that link the metamorphic and tectonic histories of the Gran Paradiso and Monte Rosa nappes (e.g., Dal Piaz and

Lombardo 1986, and references therein). Moreover, our ages overlap estimates for the HP-UHP metamorphism in the Zermatt-Saas ophiolite. The UHP units from Lago di Cignana are among the structurally highest units in the Zermatt-Saas ophiolite and U–Pb zircon ages of 44.1 ± 0.7 (Rubatto et al. 1998), a Sm–Nd age of 40.6 ± 2.6 (Amato et al. 1999), and a Lu–Hf age of 48.8 ± 2.1 (Lapen et al. 2003) are collectively interpreted to reflect a period of prograde metamorphism from ~50 to 38 Ma, where peak eclogite-facies metamorphism occurred between ~40 and 38 Ma (Lapen et al. 2003). In structurally lower sections of the Zermatt-Saas at St Jacques, a Sm–Nd isochron that used garnet cores produced an age of 50.4 ± 4.0 Ma (Mayer et al. 1999). Based on these ages, it seems likely that the Zermatt-Saas ophiolite experienced a protracted prograde history and possibly diachronous peak eclogite-facies metamorphism.

P–T–t history of the Monte Rosa nappe

Pressure and temperature conditions of Alpine high-P metamorphism are generally consistent across the Monte Rosa nappe, ranging from 450 to 600°C and >1.3 GPa (Frey et al. 1976; Dal Piaz and Lombardo 1986; Borghi et al. 1996; Engi et al. 2001a; this study). However, higher pressures of 1.6 (Chopin and Monié 1984) and 2.5 GPa (Le Bayon et al. 2000) have been interpreted from phengite-talc-chloritoid-kyanite whiteschsits within granitic orthogneiss of the Monte Rosa nappe (Lange et al. 2000). These *P–T* conditions are consistent with, but are generally lower in pressure than the conditions recorded in the HP (P = 1.8–2.0 GPa; e.g., Barnicoat and Fry 1986; Cartwright and Barnicoat 2002), or perhaps UHP (P > 2.7 GPa; Bucher et al. 2005), eclogites of the Zermatt-Saas ophiolite complex.

If we assume that the maximum *P–T* conditions in the study area are 480–570°C and >1.3–1.4 GPa, as defined by the eclogite boudins (Dal Piaz and Lombardo 1986; this study), the 42.6 ± 0.6 Ma U–Pb rutile ages record near-peak *P–T* conditions. This age does not represent a cooling age because the closure temperature for Pb in rutile is significantly greater that the peak metamorphic temperatures of the Monte Rosa nappe (e.g., Cherniak 2000; Vry and Baker 2006). Figure 9 shows the *P–T* data for the eclogites studied here, as well as the *P–T* trajectory inferred for the Monte Rosa nappe by Borghi et al. (1996). Emplacement of the quartz–carbonate–white mica–rutile veins into the host eclogite at 42.6 Ma would have to occur in the stability field of omphacite, as shown by the $Jd_{41–46}$ curve in Fig. 9, because there are no indications, either as retrograde textures or changes in mineral compositions, of alteration associated with vein emplacement. It is possible, of course, that the veins were emplaced during either the prograde or retrograde leg of the HP (omphacite stable) path shown in Fig. 9. Subsequent to peak metamorphic conditions, the eclogite, veins, and surrounding schist have all undergone some degree of recrystallization to greenschist-facies mineral assemblages. Evidence for greenschist-facies recrystallization includes Ca–Na amphibole + feldspar replacement of garnet and omphacite in eclogite, titanite replacement of rutile + carbonate + quartz, as well as chlorite replacement of carbonate in veins, in addition to poikiloblastic albite + biotite + epidote (±hornblende; Borghi et al. 1996) in schist. The age of the greenschist facies (500–550°C, ≤0.5 GPa; Borghi et al. 1996) retrograde assemblages lies between 36 and 38 Ma (Hunziker and Bearth 1969; Hunziker 1970, 1974; Inger and Ramsbotham 1997; Meffan-Main et al. 2004). This in turn constrains the minimum initial exhumation rate for the Monte Rosa nappe to be >3.3 km/Ma using an average overburden density of ~2.9 g/cm^3, the age and *P–T* conditions of greenschist-facies metamor-

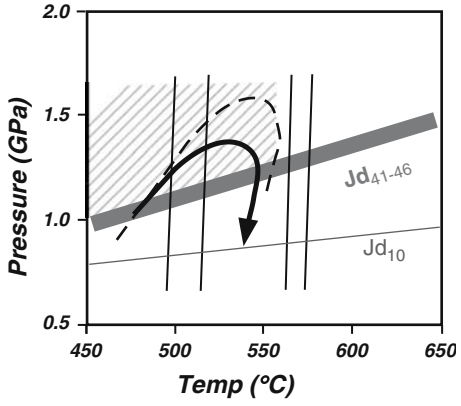

Fig. 9 Pressure-temperature diagram for the Monte Rosa nappe compiled from this and previous studies. Temperatures (*subvertical lines*) are calculated from Fe–Mg garnet-pyroxene exchange thermometer (Ravna 2000); minimum pressures of eclogite-facies metamorphism are determined by the jadeite (*Jd*) content of clinopyroxene in the absence of feldspar (Holland 1983; Gasparik 1985). The *solid black* curve with an *arrow* represents the *P–T* path of the Monte Rosa nappe as determined by Borghi et al. (1996) from mineral assemblages in pelitic components of the Monte Rosa nappe, including assemblages near Stollemberg (Fig. 2); the *dashed line* represents the *P–T* path inferred if the Monte Rosa nappe experienced peak pressures of 1.6 GPa (Chopin and Monié 1984). Higher pressures of 2.5 GPa have been documented in talc-chloritoid whiteschists of the Monte Rosa nappe by Le Bayon et al. (2000). Pressures determined by Borghi et al. (1996) and Chopin and Monié (1984) may therefore be minimum estimates. The *gray hatched* area represents the range in temperatures recorded by quartz–rutile oxygen isotope thermometry of the veins in equilibrium with eclogite-facies minerals

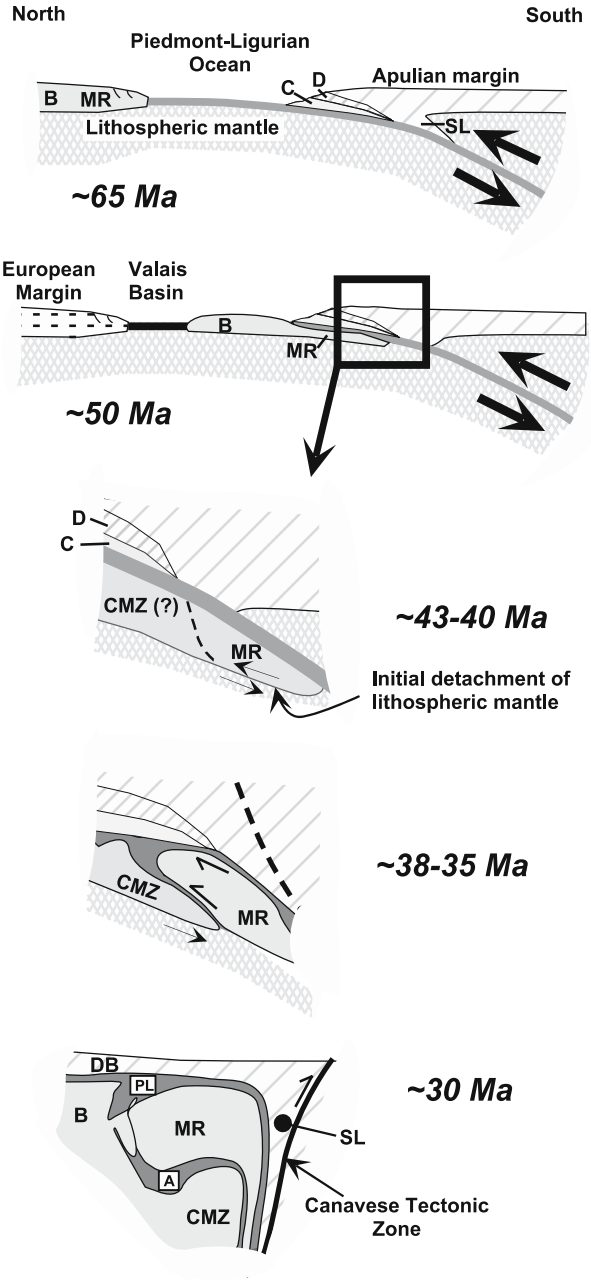

Fig. 10 Schematic NW–SE cross-section across the Alpine orogen from the Late Cretaceous to the Oligocene. In this model, the Monte Rosa nappe (*MR*) ultimately originated from the ocean-facing European passive continental margin (e.g., Compagnoni et al. 1977; Dal Piaz and Ernst 1978; Beccaluva et al. 1984; Dal Piaz 1999). *Dark gray*: oceanic crust of the Piedmont-Ligurian Ocean (basin widths and crustal thicknesses are not shown to scale); **d** Dent Blanche nappe system; **c** ophiolitic Combin zone. At ~65 Ma, rocks from the Adriatic margin were subducted to blueschist-facies (Pillonet klippe, Dent Blanche system) and eclogite-facies (Sesia-Lanzo zone) metamorphic conditions. Continued subduction and closure of the Piedmont-Ligurian Ocean basin occurred through 50 Ma; the black crust represents the Valais oceanic basin (the age of its opening is unknown). Note that at 42 Ma, the Monte Rosa nappe and Zermatt-Saas ophiolite (*dark gray crust*) are linked because of their very similar HP *P–T* history. Also during this time period, the Monte Rosa has decoupled from its lithospheric mantle. By 38–35 Ma, the Austroalpine-inner Penninic collisional wedge, just accreted by the blueschist-facies Grand St. Bernhard nappe system (**b**) and the Antrona ophiolite (**a**), essentially equivalent to oceanic rocks of the Piemont-Ligurian Ocean (*PL*), experienced the post-nappe greenschist-amphibolite facies metamorphic overprint. The Camughera-Moncucco zone (*CMZ*) is interpreted as the inner edge of the Bernhard nappe (**b**). By 30, the inner part of the collisional wedge was mainly exhumed, cooled, fractured and transected by andesitic-lamproitic dykes of 30 Ma (Venturelli et al. 1984), not shown in the figure. Later, the collisional wedge was indented by the Southalpine lithosphere

phism of the Gran Paradiso and Monte Rosa nappes, and the *P–T* conditions of ≥1.3 GPa and 570°C at 42.6 Ma. Although this is a minimum rate for the Monte Rosa, it is much slower than the 25–34 km/Ma exhumation rate that is inferred for the UHP units in the western Alps (Amato et al. 1999; Rubatto and Hermann 2001).

Implications for exhumation mechanisms of HP rocks in the western Alps

The 42.6 Ma age for eclogite-facies metamorphism in the Monte Rosa nappe and the 43 Ma age for peak, eclogite-facies metamorphism in the Gran Paradiso nappe (Meffan-Main et al. 2004), combined with the ~50–38 Ma period of prograde metamorphism of UHP rocks within the structurally overlying Zermatt-Saas ophiolite (Lago di Cignana; Lapen et al. 2003), suggests that these continental and oceanic units were buried at the same time (Fig. 10). Underthrusting of the Internal Penninic continental basement nappes below the Zermatt-Saas ophiolite during subduction is consistent with the present structural configuration of the western Alps (e.g., Dal Piaz and Ernst 1978; Dal Piaz 1999, and references therein; Dal Piaz et al. 2001; Froitzheim 2001; Meffan-Main et al. 2004; Fig. 10). The overall range in pressure and temperature of the Zermatt-Saas ophiolite north of the Aosta-Ranzola fault (Fig. 1) is fairly restricted (550–600°C, 1.7–2.0 GPa; Barnicoat and Fry 1986), with the exception of the coesite-bearing eclogite at Lago di Cignana (Reinecke 1991). If the >1.7 GPa pressures recorded in whiteschists of the Monte Rosa nappe represent the true peak pressure of this unit (Chopin and Monié 1984; Le Bayon et al. 2000), the present age and *P–T* data sets are consistent with an interpretation that the Monte Rosa and Gran Paradiso nappes were accreted to and coupled with sections of the Zermatt-Saas ophiolite at eclogite-facies conditions. Furthermore, because decompression and cooling in these basement nappes are essentially coeval with decompression and cooling in the Zermatt-

Saas ophiolite, it seems to us that it is very probable that these units were coupled with one another over much of their exhumation history as well (e.g., Escher and Beaumont 1997).

Most large, eclogite-facies terranes that occur in the upper crust are associated with low-density lithologies such as serpentinite (~2.6 g/cc) and/or subducted continental material (~2.7–3.0 g/cc; Ernst et al. 1997; Schwartz et al. 2001), and it is therefore probable that the presence of these materials play a very important role in exhumation of eclogitic rocks. Could the continental basement nappes in the western Alps have been, in conjunction with serpentinite associated with the Zermatt-Saas ophiolite, responsible for 'saving' a tract of ocean crust from its ultimate demise in the mantle? If the oceanic and continental units behaved, in general, as a coherent tectonic nappe during exhumation (e.g., Escher and Beaumont 1997), models involving simultaneous normal- and reverse-sense motion occurring along upper and lower bounding shears (e.g., Dal Piaz et al. 1972; Wheeler 1991; Escher and Beaumont 1997; Meffan-Main et al. 2004) can be invoked for a composite Zermatt-Saas/Monte Rosa–Gran Paradiso unit. This model is supported in the Monte Rosa area by the presence of an upper-bounding greenschist-facies, normal-sense shear zone, which separates footwall eclogite-facies rocks (Monte Rosa nappe and Zermatt-Saas ophiolite) from hanging-wall blueschist/greenschist-facies rocks (Combin zone; Ballèvre and Merle 1993; Reddy et al. 1999, 2003). A lower-bounding reverse-sense shear zone situated between the Monte Rosa upper plate and the lower plate of the Antrona ophiolite is inferred by Ring and Merle (1992), Escher and Beaumont (1997), Escher et al. (1997), and Keller (2004). The relative displacements along the basal reverse-sense shear zone were likely accommodated by buoyancy assisted upward movements of the Monte Rosa nappe and underplating of the Antrona ophiolite and Grand St Bernhard system. We conclude that coupling of continental and oceanic terranes were a general feature in the western Alps that aided uplift of the eclogite units.

Conclusions

High-precision U–Pb geochronology of rutile from quartz–carbonate–white mica–rutile veins that formed during eclogite-facies metamorphism indicates that the Monte Rosa nappe was at eclogite-facies metamorphic conditions at 42.6 ± 0.6 Ma. The timing of eclogite-facies metamorphism in the Monte Rosa nappe is identical to that of the Gran Paradiso nappe (Meffan-Main et al. 2004), confirming that these two units shared the same Alpine metamorphic history. The nearly identical *P–T–t* histories of the Gran Paradiso and Monte Rosa nappes and the same timing of eclogite-facies metamorphism as Zermatt-Saas ophiolite indicates that these units shared much of their Alpine tectonic and metamorphic histories. The tectono-metamorphic evolution of these oceanic and continental nappes mainly developed inside the Austroalpine-Penninic wedge that maintained its subduction-related cool thermal regime during syn-collisional subduction of the European passive margin, tectonic off-scraping, and subsequent wedge accretion. The close association between HP ophiolite and continental crust suggests that the HP internal basement nappes in the western Alps may have aided in the exhumation of the ophiolitic rocks, and in fact, such associations may be critical to preventing permanent loss of subducted ophiolitic rocks to the mantle.

Acknowledgments This research was supported by National Science Foundation grant EAR 0309853 (CMJ), the U.W. Madison Morgridge Graduate Fellowship (TJL), the Geological Society of America (TJL), and a summer research grant from the Department of Geology and Geophysics, U.W. Madison. We thank Benita Putliz for her assistance with the oxygen isotope analyses as well as Andrew Hein and Nancy Mahlen for their assistance in the field. Journal reviews were provided by Kurt Bucher and an anonymous reviewer.

References

Agrinier P (1991) The natural calibration of $^{18}O/^{16}O$ geothermometers; application to the quartz-rutile mineral pair. Chem Geol 91:49–64

Amato JM, Johnson CM, Baumgartner LP, Beard BL (1999) Rapid exhumation of the Zermatt-Saas ophiolite deduced from high-precision Sm-Nd and Rb-Sr geochronology. Earth Planet Sci Lett 171:425–438

Armstrong JT (1988) Quantitative analysis of silicate and oxide materials: comparison of Monte Carlo, ZAF, and $\varphi(\rho z)$ procedures. In: Newbury DE (eds) Microbeam analyses, proceedings of the 23rd annual conference of the microbeam analysis society. San Francisco Press, San Francisco, CA pp 239–246

Arnaud NO, Kelley SP (1995) Evidence for excess argon during high pressure metamorphism in the Dora Maira Massif western Alps, Italy, using an ultra-violet laser ablation microprobe $^{40}Ar/^{39}Ar$ technique. Contrib Mineral Petrol 121:1–11

Ballèvre M, Kienast JR, Vuichard JP (1986) La nappe de la Dent Blanche: deux unités austroalpines indépendantes. Eclogae Geol Helv 79:57–74

Ballèvre M, Merle O (1993) The combin fault: reactivation of a detachment fault. Schweiz Mineral Petrogr Mitt 73:205–227

Barnicoat AC, Fry N (1986) High-pressure metamorphism of the Zermatt-Saas ophiolite zone, Switzerland. J Geol Soc Lond 143:607–618

Beccaluva L, Dal Piaz GV, Macciotta G (1984) Transitional to normal-MORB affinities in ophiolitic metabasites from the

Zermatt-Saas, Combin and Antrona units, western Alps: implications for the paleogeographic evolution of the western Tethyan basin. Geol Mijnbow 63:165–177
Bearth P (1952) Geologie und petrography des Monte Rosa. Beitr Geol Karte Schweiz 96:94
Bearth P (1958) Uber einen Wechsel der Mineral-fazies in der Wurzelsone des Penninikums. Schweiz Mineral Petrogr Mitt 38:363–373
Bigi G, Castellarin A, Coli M, Dal Piaz GV, Sartori R, Scandone P, Vai GB (1990) Structural model of Italy, 1:500.000, Sheet 1. C.N.R., Progetto Finalizzato Geodinamica, SELCA Firenze
Bistacchi A, Dal Piaz G, Massironi M, Zattin M, Balestrieri M (2001) The Aosta-Ranzola extensional fault system and oligocene-present evolution of the Austroalpine-Penninic wedge in the northwestern Alps. Int J Earth Sci 90:654–667
Bocquet J, Delaloye M, Hunziker JC, Krummenaker D (1974) K-Ar and Rb-Sr dating of blue amphiboles, micas and associated minerals from the western Alps. Contrib Mineral Petrol 47:7–26
Borghi A, Compagnoni R, Sandrone R (1996) Composite P-T paths in the internal Penninic massifs of the western Alps: petrological constraints to their thermo-mechanical evolution. Eclog Geol Helv 89/1:345–367
Bowtell SA, Cliff RA, Barnicoat AC (1994) Sm-Nd isotopic evidence on the age of eclogitization in the Zermatt-Saas ophiolite. J Metamorph Geol 12:187–196
Bucher K, Fazis Y, de Capitani C, Grapes R (2005) Blueschists, eclogites and decompression assemblages of the Zermatt-Saas ophiolite: high-pressure metamorphism of subducted Tethys lithosphere. Am Mineral 90:821–835
Bussy F, Eichenberger M, Giroud N, Masson H, Meilhac C, Presniakov S (2005) Early Carboniferous age of the Versoyen magmatism and consequences: non-existence of a Valais Ocean in the western Alps. Third Swiss Geoscience Meeting, Zurich
Carswell DA, Brueckner HK, Cuthbert SJ, Mehta K, O'Brian PJ (2003) The timing of stabilisation and the exhumation rate for ultra-high pressure rocks in the Western Gneiss region of Norway. J Metamorphic Geol 21:601–612
Cartwright I, Barnicoat AC (2002) Petrology, geochronology, and tectonics of Shear Zones in the Zermatt-Saas and Combin Zones of the western Alps. J Metamorphic Geol 20:263–281
Cherniak DJ (2000) Pb diffusion in rutile. Contrib Mineral Petrol 139:198–207
Chopin C (1984) Coesite and pure pyrope in high-grade blueschists of the western Alps: a first record and some consequences. Contrib Mineral Petrol 86:107–118
Chopin C, Maluski H (1980) 40Ar-39Ar dating of high-pressure metamorphic micas from the Gran Paradiso area (western Alps): evidence against the blocking-temperature concept. Contrib Mineral Petrol 74:745–749
Chopin C, Monié P (1984) A unique magnesiochloritoid-bearing, high-pressure assemblage from the Monte Rosa, western Alps: petrological and $^{40}Ar/^{39}Ar$ radiometric study. Contrib Mineral Petrol 87:388–398
Compagnoni R, Dal Piaz GV, Hunziker JC, Gosso G, Lombardo B, Williams PF (1977) The Sesia-Lanzo zone, a slice of continental crust with Alpine high pressure-low temperature assemblages in the Western Italian Alps. Rend Soc It Min Petr 33:281–334
Cortiana G, Dal Piaz GV, Del Moro A, Hunziker JC, Martin S (1998) 40Ar/39Ar and Rb-Sr dating of the Pillonet klippe and Sesia-Lanzo basal slice in the Ayas valley and evolution of the Austroalpine-Piedmont nappe stack. Mem Soc Geol Ital 50:177–194
Coward M, Dietrich D (1989) Alpine tectonics—an overview. In: Coward MP, Dietrich D, Park RG (eds) Alpine tectonics. Geol Soc Spec Publ 45:1–33
Dal Piaz GV (1971) Nuovi ritrovamenti di cianite alpine nel cristallino antico del Monte Rosa. Rend Soc It Min Petr 27:437–477
Dal Piaz GV (1993) Evolution of Austro-Alpine and Upper Penninic basement in the northwestern Alps from Variscan convergence to post-Variscan extension. In: Von Raumer J, Neubauer F (eds) Pre-Mesozoic geology in the Alps. Springer-Verlag, New York, pp 327–344
Dal Piaz GV (1999) The Austroalpine-Piedmont nappe stack and the puzzle of Alpine Tethys. Mem Sci Geol Padova 51(1):155–176
Dal Piaz GV (2001) Geology of the Monte Rosa massif: historical review and personal comments. Schweiz Mineral Petrogr Mitt 81:275–303
Dal Piaz GV, Bistacchi A, Massironi M (2003) Geological outline of the Alps. Episodes 26(3):175–180
Dal Piaz GV, Hunziker JC, Martinotti G (1972) La zona Sesia-Lanzo e l'evoluzione tettonico-metamorfica delle Alpi nordoccidentali interne. Mem Soc Geol It 11:433–466
Dal Piaz GV, Gatto G (1963) Considerazioni geologico-petrografiche sul versante meridionale del Monte Rosa. Rend Acc Naz Lincei Cl Sci Fis 34:190–194
Dal Piaz GV, Cortiana G, Del Moro A, Martin S, Pennacchioni G, Tartarotti P (2001) Tertiary age and paleostructural inferences of the eclogitic imprint in the Austroalpine outliers and Zermatt-Saas ophiolite, western Alps. Int J Earth Sci 90:668–684
Dal Piaz GV, Ernst WG (1978) Areal geology and petrology of eclogites and associated metabasites of the Piemonte ophiolite nappe, Breuil-St. Jacques area, Italian western Alps. Tectonophysics 51:99–126
Dal Piaz G, Lombardo B (1986) Early Alpine eclogite metamorphism in the Penninic Monte Rosa-Gran Paradiso basement nappes of the northwestern Alps. Geol Soc Am Mem 164:249–265
Darbellay B (2005) Polymetamorphism history of the Monte Rosa nape and isotopic constraints, Val d'Ayas, Italy. Master's Thesis, University of Lausanne, Lausanne, Switzerland
Droop GTR (1987) A general equation for estimating Fe^{3+} concentrations in ferromagnesian silicates and oxides from microprobe analysis, using stoichiometric criteria. Mineral Mag 51:431–435
Engi M, Scherrer N, Burri T (2001a) Metamorphic evolution of pelitic rocks of the Monte Rosa nappe: constraints from petrology and single grain monazite age data. Schweiz Mineral Petrogr Mitt 81:305–328
Engi M, Berger A, Roselle GT (2001b) Role of the tectonic accretion channel in collisional orogeny. Geology 29:1143–1146
Ernst WG (1971) Metamorphic zonation of presumably subducted lithospheric plates from Japan, California and the Alps. Contrib Mineral Petrol 34:43–59
Ernst WG, Maruyama S, Wallis S (1997) Buoyancy-driven, rapid exhumation of ultrahigh-pressure metamorphosed continental crust. Proc Natl Acad Sci 94:9532–9537
Escher A, Beaumont C (1997) Formation, burial and exhumation of basement nappes at crustal scale: a geometric model based on the western Swiss-Italian Alps. J Struct Geol 19(7):955–974
Escher A, Hunziker JC, Marthaler M, Masson H, Sartori M, Steck A (1997) Geologic framework and structural evolution of the Western Swiss-Italian Alps. In: Pfiffner OA,

Lehner P, Heitzman P, Mueller S, Steck A (eds) Deep structure of the Swiss Alps. Results of NRP 20. Birkhäuser Verlag, Basel, pp 223–239

Ferrando J (2002) Evoluzione tettonica e metamorfica delle eclogiti incluse nella crosta continentale del Monte Rosa. Unpublished Thesis, Fac. Science, University Genova, Genova, Italy

Ferrando J, Scambelluri M, Dal Piaz GV, Piccardo GB (2002) The mafic boudins of the southern Furgg-Zone, Monte Rosa nappe, NW-Italy: from tholeiitic continental basalts to Alpine eclogites and retrogressed products. 81 Riunione Estiva Soc. Geol. It., Torino 10–12 September 2002 (abstract)

Frey M, Hunziker JC, Frank W, Bocquet J, Dal Piaz GV, Jäger E, Niggli E (1974) Alpine metamorphism of the Alps: a review. Schweiz Mineral Petrogr Mitt 54:247–290

Frey M, Hunziker JC, O'Niel JR, Schwander HW (1976) Equilibrium-disequilibrium relations in the Monte Rosa granite, western Alps: petrological, Rb-Sr, and stable isotope data. Contrib Mineral Petrol 55:147–179

Froitzheim N (2001) Origin of the Monte Rosa nappe in the Pennine Alps—a new working hypothesis. GSA Bulletin 113(5):604–614

Gosso G, Dal Piaz GV, Piovano V, Polino R (1979) High pressure emplacement of early-alpine nappes, postnappe deformations and structural levels (internal northwestern Alps). Mem Sci Geol 32:16

Hacker BR, Calvert AT, Zhang RY, Ernst WG, Liou JG (2003) Ultra-rapid exhumation of ultrahigh pressure diamond-bearing metasedimentary rocks of the Kokchetav Massif Lithos 70:61–75

Holland TJB (1983) The experimental determination of activities in disordered and short-range ordered jadeitic pyroxenes. Contrib Mineral Petrol 82(2):214–240

Hunziker JC (1970) Polymetamorphism in the Monte Rosa, western Alps. Eclogae Geol Helv 63:151–161

Hunziker JC (1974) Rb-Sr and K-Ar age determination and the alpine tectonic history of the western Alps, vol 31. Memoir Ist. Mineral. Petrogr. Univ. Padova, Padova, Italy, pp 1–55

Hunziker JC, Bearth P (1969) Rb-Sr Altersbestimmungen aus den Walliser-Alpen: biotitalterswerte und ihre Bedeutung für die Abkühlungsgeschichte der alpinen metamorphose. Eclogae Geol Helv 62:205–222

Hunziker JC, Desmons J, Hurford AJ (1992) Thirty-two years of geochronological work in the Central and western Alps: a review on seven maps. Mémoires de Géologie (Lausanne), 59 pp

Hurford AJ, Hunziker JC (1989) A revised thermal history for the Gran Paradiso massif. Schweiz Mineral Petrogr Mitt 69:319–329

Hurford AJ, Hunziker JC, Stöckhert B (1991) Constraints on the late thermotectonic evolution of the western Alps: evidence for episodic rapid uplift. Tectonics 10(4):758–769

Inger S, Ramsbotham W, Cliff RA, Rex DC (1996) Metamorphic evolution of the Sesia Lanzo Zone, western Alps: time constraints from multi-system geochronology. Contrib Mineral Petrol 126:152–168

Inger S, Ramsbotham W (1997) Syn-convergent exhumation implied by progressive deformation and metamorphism in the Valle del'Orco transect, NW Italian Alps. J Geol Soc 154:667–677

Gasparik T (1985) Experimentally determined compositions of diopside-jadeite pyroxene in equilibrium with albite and quartz at 1200-1350 degrees C and 15-34 kbar. Geochim Cosmochim Acta 49:865–870

Ghent ED (1988) A review of chemical zoning in eclogite garnets. In: Smith DC (eds) Eclogites and Eclogite-Facies Rocks. Elsevier, Amsterdam, pp 207–236

Gosso G, Dal Piaz GV, Piovano V, Polino R (1979) High pressure emplacement of early-Alpine nappes, postnappe deformations and structural levels. Mem Sci Geol 32:15

Johnson CM, Beard BL (1999) Correction of instrumentally-produced mass fractionation during isotopic analysis of Fe by thermal ionization mass spectrometry. Int J Mass Spectrom 193:87–99

Keller LM (2004) Relationships between metamorphism and deformation: examples on the micro- to macro-scale from the western Alps. PhD Dissertation, University of Basel, Basel

Kurz W, Froitzheim N (2002) The exhumation of eclogite-facies metamorphic rocks; a review of models confronted with examples from the Alps. Int Geol Rev 44:702–743

Lapen TJ, Johnson CM, Baumgartner LP, Mahlen NJ, Beard BL, Amato J (2003) Burial rates during prograde metamorphism of an ultra-high-pressure terrane: an example from Lago di Cignana, western Alps, Italy. Earth Planet Sci Lett 215:57–72

Lange S, Nasdala L, Poller U, Baumgartner LP, Todt W (2000) Crystallization age and metamorphism of the Monte Rosa granite, western Alps. Seventeenth Swiss Tectonic Studies Group Meeting, Zürich, p51

Lardeaux JM, Spalla MI (1991) From granulites to eclogites in the Sesia zone (Italian western Alps): a record of the opening and closure of the Piedmont Ocean. J Metamorphic Geol 9:35–59

Le Bayon R, de Capitani C, Chopin C, Frey M (2000) Modeling of the sequential evolution of whiteschist assemblages: HP in the Monte Rosa (western Alps). Beih Eur J Min 12:111

Liati A, Gebauer D, Froitzheim N, Fanning MC (2001) U-Pb SHRIMP geochronolgy of an amphibolitized eclogite and an orthogneiss from the Furgg zone (western Alps) and implications for its geodynamic evolution. Schweiz Mineral Petrogr Mitt 81:379–393

Ludwig KR (1980) Calculation of uncertainties of U-Pb isotope data. Earth Planet Sci Lett 46:212–220

Ludwig KR (2001) User's manual for Isoplot/Ex rev.2.49, a geochronological toolkit for Microsoft Excel. Berkeley Geochronol Center Spec Publ 1a:59

Matthews A (1994) Oxygen isotope geothermometers for metamorphic rocks. J Metamorphic Geol 12:211–219

Mayer A, Abouchami W, Dal Piaz GV (1999) Eocene Sm-Nd age for the eclogitic metamorphism of the Zermatt-Saas ophiolite in Ayas Valley, western Alps. Eur Union Geosci 10:809 (abstract)

Meffan-Main S, Cliff RA, Barnicoat AC, Lombardo B, Compagnoni R (2004) A Tertiary age for Alpine high-pressure metamorphism in the Gran Paradiso Massif, western Alps; a Rb-Sr microsampling study. J Metamorphic Geol 22:261–281

Michard A, Goffé B, Chopin Ch, Henry C (1996) Did the western Alps develop through an Oman-type stage? Eclogae Geol Helv 89:43–80

Oberhänsli R et al (eds) (2004) Metamorphic structure of the Alps and explanatory notes. Mitt Oesterr Min Ges 149:115–226

Paquette JL, Chopin C, Peucat JJ (1989) U-Pb zircon, Rb-Sr, and Sm-Nd geochronology of high- to very-high-pressure metaacidic rocks from the western Alps. Contrib Mineral Petrol 101:280–289

Pawlig S, Baumgartner LP, Hauzenberger CA (2001) Geochemistry of a talc-chloritoid-kyanite shear zone within the Monte Rosa granite, Val d'Ayas, Italy. In: Engi M,

Nievergelt P (eds) Contributions to the geology of the Monte Rosa Nappe. Schweiz Mineral Petrogr Mitt 81(3):329–346

Pfiffner OA, Lehner P, Heitzman PZ, Mueller S, Steck A (1997) Deep structure of the Swiss Alps—results from NRP 20. BirkhaYser AG, Basel, 380p

Ravna EKJ (2000) The garnet-clinopyroxene geothermometer, an updated calibration. J Metamorphic Geol 18:211–219

Reddy SM, Wheeler J, Cliff RA (1999) The geometry and timing of orogenic extension: an example from the western Italian Alps. J Metamorph Geol 17:573–589

Reddy SM, Wheeler J, Butler RWH, Cliff RA, Freeman S, Inger S, Pickles C, Kelly SP (2003) Kinematic reworking and exhumation within the convergent Alpine orogen. Tectonophysics 365:77–102

Reinecke T (1991) Very high–pressure metamorphism and uplift of coesite-bearing metasediments from the Zermatt-Saas zone, western Alps. Eur J Mineral 3:7–17

Ring U, Merle O (1992) Forethrusting, backfolding, and lateral gravitational escape in the northern part of the western Alps (Monte Rosa region). Bull Geol Soc Am 104:901–914

Roure F, Heitzmann P, Polino R (eds) (1990) Deep structure of the Alps. Mem Soc Geol Fr 156:1–367

Rubatto D, Gebauer D (1999) Eo/Oligocene (35 Ma) high-pressure metamorphism in the Gornergrat zone (Monte Rosa, western Alps): implications for paleogeography. Schweiz Mineral Petrogr Mitt 79:353–362

Rubatto D, Gebauer D, Fanning M (1998) Jurassic formation and Eocene subduction of the Zermatt-Saas Fee ophiolites: implications for the geodynamic evolution of the central and western Alps. Contrib Mineral Petrol 132:269–287

Rubatto D, Hermann J (2001) Exhumation as fast as subduction? Geology 29(1):3–6

Ruffet G, Gruau G, Ballevre M, Feraud G, Philippot P (1997) Rb–Sr and $^{40}Ar/^{39}Ar$ laser probe dating of high-pressure phengites from the Sezia zone, western Alps: underscoring of excess argon and new age constraints on the high-pressure metamorphism. Chem Geol Isot Geosci Sect 141:1–18

Schwartz S, Allemand P, Guillot S (2001) Numerical model of the effect of serpentinites on the exhumation of eclogitic rocks: insights from the Monviso ophiolitic massif (western Alps). Tectonophysics 342:193–206

Sharp ZD (1992) In situ laser microprobe techniques for stable isotope analysis. Chemical Geol 101:3–19

Spalla IM, Lardeaux JM, Dal Piaz GV, Gosso G, Messiga B (1996) Tectonic significance of Alpine eclogites. J Geodynamics 21:257–285

Stampfli GM, Marchant RH (1997) Geodynamic evolution of the Tethyan margins of the western Alps. In: Pfiffner OA, Lehner P, Heitzman P, Mueller S, Steck A (eds) Deep structure of the Swiss Alps. Results of NRP 20. Birkhäuser Verlag, Basel, pp 223–239

Venturelli G, Thorpe RS, Dal Piaz GV, Del Moro A, Potts PJ (1984) Petrogenesis of calcalcaline, shoshonitic and associated ultrapotassic Oligocene volcanic rocks from the Northwestern Alps, Italy. Contrib Mineral Petrol 86:209–220

Vry JK, Baker JA (2006) LA-MC-ICPMS Pb-Pb dating of rutile from slowly cooled granulites: confirmation of the high closure temperature for Pb diffusion in rutile. Geochim Cosmochim Acta 70:1807–1820

Wheeler J (1991) Structural evolution of a subducted continental sliver: the northern Dora Maira massif, Italian Alps. J Geol Soc Lond 148:1101–1113